Deciphering Breast Cancer Complexity: A Study on the Predictive Power of MRI Texture Analysis for Tumor Characterization and Treatment Response

Hamza Eren Güzel[1], Ali Murat Koç[2], Zehra Hilal Adıbelli[1], Funda Alkan Taşlı[3], Babak Saravi[4]

[1]Department of Radiology, University of Health Sciences, Izmir Bozyaka Training and Research Hospital, Izmir, Turkey
[2]Department of Radiology, Atatürk Education and Research Hospital, Izmir Katip Celebi University, Izmir, Turkey
[3]Department of Pathology, University of Health Sciences, Izmir Bozyaka Training and Research Hospital, Izmir
[4]Department of Orthopedics and Trauma Surgery, Faculty of Medicine, Medical Center - University of Freiburg, University of Freiburg, Freiburg, Germany
Email: hamzaerenguzel@gmail.com

Abstract

This study examined the association between MRI radiomics features of malignant breast masses and their histopathological, molecular characteristics, and response to neoadjuvant treatments. Utilizing a retrospective cohort of 70 breast cancer patients, this study conducted a detailed texture analysis on preoperative MRI scans, including the extraction of texture features, such as entropy, contrast, and homogeneity, and their analysis against histopathological and clinical target variables (e.g., lymph node metastasis) and molecular profiles. Statistical analyses and machine learning algorithms, including logistic regression and support vector machines, were employed to evaluate the predictive power of MRI texture features for determining molecular subtypes and evaluate the association of radiomics markers with neoadjuvant treatments. The findings reveal significant associations between specific MRI texture features and the histopathological and molecular characteristics of breast tumors, demonstrating that certain texture parameters are strongly associated with aggressive tumor phenotypes and poorer response to chemotherapy. Despite the limited dataset, machine learning models showcased promising performance in classifying tumors into molecular subtypes and predicting treatment outcomes, highlighting the potential of MRI texture analysis in clinical decision-making. This study underscores the potential of MRI texture analysis as a non-invasive tool for enhancing the personalized management of breast cancer. The significant associations between MRI texture features and critical tumor characteristics suggest that these features could serve as valuable biomarkers for predicting tumor behavior and treatment efficacy. The findings advocate for further large-scale research into integrating MRI texture analysis into clinical practice to tailor treatment strategies to individual tumor profiles, ultimately aiming to improve patient outcomes in breast cancer treatment.

Keywords: breast cancer; texture analysis; breast mri; neoadjuvant therapy; cancer subtypes; tumor heterogeneity.

Recent statistics have positioned female breast cancer as the foremost cause of cancer incidence globally in 2020 [1]. With approximately 2.3 million new cases, it constitutes 11.7% of total cancer cases, making it the most frequently diagnosed cancer in women and the primary cause of cancer-related deaths among them. This disease accounts for a quarter of all cancer cases and a sixth of cancer deaths in women, leading in incidence in most countries [1]. Notably, its incidence rates in women are significantly higher than other cancers, with 55.9 per 100,000 in developed countries and 29.7 per 100,000 in developing countries [1]. The global response to this alarming trend includes extensive breast cancer screening programs, aimed at decreasing mortality rates through early detection and timely treatment [2]. Diagnostic breast imaging serves a dual purpose: it is utilized for screening in women without symptoms to facilitate early identification of breast cancer and is also employed to investigate breast abnormalities in symptomatic women, aiding in the timely detection of this disease. The World Health Organization advocates for regular, organized mammography screenings every two years for women aged 50 to 69 who are at average risk, particularly in resource-rich settings [3].

Conventional mammography, typically comprising bi-planar projections, is the cornerstone of screening modalities. In contrast, diagnostic evaluations incorporate advanced imaging techniques such as specialized mammographic views, ultrasonography (USG), and magnetic resonance imaging (MRI). MRI demonstrates a notable diagnostic accuracy for invasive breast carcinomas, with its sensitivity spanning from 75.2% to 100% and specificity ranging between 83% and 98.4% [4]. Dynamic contrast-enhanced MRI transcends mere lesion detection; it provides a comprehensive analysis encompassing lesion morphology, contour characteristics, volumetric assessment, diffusion limitations, and patterns of contrast uptake. Contemporary research underscores the significant role of these parameters in differentiating benign from malignant entities and prognosticating the histopathological attributes of the identified lesions [5–7].

Radiomics, an emerging field in medical imaging, harnesses the power of advanced computational techniques to extract a plethora of quantitative data from routine medical images [8]. This approach, predominantly applied in oncology, offers a distinct advantage over traditional biopsy methods. It allows for a comprehensive, non-invasive analysis of the entire tumor phenotype across multiple lesions simultaneously, in stark contrast to biopsies which sample only a fraction of a single heterogeneous tumor [9,10]. This ability to not only delineate but also link tumor characteristics to underlying biological processes [11] paves the way for personalized treatment strategies [12–14], aligning with the ethos of precision medicine. In breast cancer diagnostics, radiomics has demonstrated its potential in various domains including tumor diagnosis [15,16], response prediction to therapeutic interventions [17–19], molecular subtype identification [20,21], and even in forecasting axillary lymph node metastases [22,23]. The traditional diagnostic regimen for early invasive breast cancer predominantly relies on radiological

evaluations such as mammography, ultrasound, and contrast-enhanced MRI, supplemented by histopathological confirmation from tissue samples obtained radiologically [24,25]. However, this approach has limitations: suboptimal sensitivity and predictive value [26], the invasive and uncomfortable nature of biopsies, prolonged waiting times for results [27], and the potential for missing significant heterogenous features of breast cancer [28]. In the era of personalized medicine, where timely and accurate diagnosis is paramount, radiomics offers a groundbreaking alternative. By extracting and analyzing qualitative and quantitative data from imaging, it supports evidence-based clinical decision-making [29]. The integration of high-dimensional radiomic data with clinical information facilitates the creation of robust decision support models. Thus, radiomics emerges not just as a diagnostic tool, but as a comprehensive approach for molecular profiling and treatment response assessment in breast cancer, potentially minimizing the need for invasive procedures [29].

The primary objective of our study is to meticulously compare the texture characteristics derived from MRI of known malignant breast masses with their corresponding histopathological and molecular features, as well as their response to neoadjuvant treatments. By identifying associations between these variables, our research aims to assess the utility of MRI texture features as reliable indicators of intratumoral heterogeneity. This endeavor could significantly contribute to predicting pathological outcomes and neoadjuvant responses, thereby advancing the field of personalized breast cancer management.

Materials and Methods

2.1. Study Design and Population

This study was conducted in the Department of Radiology, Health Sciences University Izmir Bozyaka Training and Research Hospital, spanning the period from October 7, 2020, to January 10, 2021. Ethical approval was granted by the Clinical Research Ethics Committee of the same institution (Approval No: 07, Dated: October 7, 2020), approving the retrospective nature of this investigation.

Our research centered on patients diagnosed with breast cancer within the Department of Pathology, Health Sciences University Izmir Bozyaka Training and Research Hospital, over the years 2018 and 2019. The study's inclusion criteria were meticulously defined to encompass: 1) individuals with a histopathological confirmation of breast carcinoma; 2) patients who underwent surgical intervention for breast cancer at our facility subsequent to their diagnosis; 3) patients who had preoperative breast MRI scans conducted at our institution; and 4) patients with lesions amenable to texture analysis on MRI, specifically those measuring at least 1 cm in diameter. Following these criteria, a cohort of 70 eligible cases was included for the study.

For each case, detailed morphological and molecular data pertaining to the breast masses were meticulously extracted from the pathology reports. Subsequently, a comprehensive texture analysis was conducted on the MRI scans of these masses, employing advanced imaging techniques to elucidate potential correlations between radiomic features and pathological findings.

2.2. Histopathological Findings and Study Variables

Histopathological analyses were performed on specimens obtained from partial or total mastectomies conducted between October 7, 2020, and January 10, 2021. Tissue samples, initially fixed in 10% formalin, were embedded in paraffin, from which 4-micron sections were prepared. These sections underwent standard Hematoxylin and Eosin staining, enabling detailed documentation of various histopathological parameters, such as histological grade and lymphovascular invasion, in the pathology reports.

Complementing the morphological assessment, a panel of immunohistochemical markers, including Estrogen Receptor (ER), Progesterone Receptor (PR), Cerb B2, P53, and Ki-67, was evaluated. These markers were processed using an automated staining system (Ventana BenchMark XT, Ventana Medical Systems, Tucson, AZ). The ensuing pathological data were meticulously recorded.

The extracted pathology report data encompassed: 1) receptor characteristics of breast carcinomas, categorized according to intrinsic subtypes (Luminal A, Luminal B, Her2 overexpression, and Triple Negative); 2) classification of intrinsic subtypes based on the status of ER, PR, Cerb B2, and Ki-67 index, with a Ki-67 cutoff value of 30% delineating low (<30%) and high (≥30%) subgroups; 3) grading of masses following the Bloom-Richardson system; 4) P53 positivity in the masses, categorized as negative (<5%), weakly positive (5-50%), and strongly positive (>50%); 5) presence of lymphovascular invasion by malignant cells; 6) detection of metastasis in dissected lymph nodes; 7) administration of neoadjuvant treatment to twenty patients pre-surgery, with their pathological responses assessed via the Miller-Payne scoring system [30]. Responses were categorized as 'no response' for grades 1-3 and 'response' for grades 4-5.

Grade	Description
1	Minimal or no cellular-level changes, with unchanged overall cell density.
2	Up to 30% reduction in tumor cell density.
3	Reduction in tumor cell density ranging from 30% to 90%.
4	Greater than 90% decrease in tumor cell density, with cells discernible individually or in small clusters.
5	Complete absence of malignant cells within the tumor bed.

Table 1: Miller-Payne Scoring System for Evaluating Pathological Response to Neoadjuvant Treatment [30].

2.3. MRI Procedure

Breast MRI examinations were performed using a 1.5 Tesla MRI system (Magnetom AERA, Siemens, Erlangen, Germany) in our clinic. To minimize hormonal influences on breast parenchyma, MRIs for premenopausal patients were strategically scheduled between the 7th and 14th days of their menstrual cycles. All examinations employed an 8-channel surface breast coil in the prone position, ensuring comprehensive coverage of a 32 cm imaging field. Prior to imaging, an antecubital vein was cannulated for the administration of the contrast agent. The contrast protocol involved the use of a gadolinium-based agent (Meglumine Gadoterat-Dotarem), dosed at 0.1-0.2 mmol/kg. Our standard breast MRI protocol encompassed a suite of sequences: initial three-plane localizer and calibration images, followed by axial fat-suppressed Turbo Spin Echo (TSE) T1-weighted (T1A) and Turbo Inversion Recovery Magnitude (TIRM) sequences, alongside T2-weighted (T2A) fat-suppressed imaging. This was

succeeded by axial pre-contrast and dynamic post-contrast T1A imaging. The dynamic component entailed T1A SPectral Attenuated Inversion Recovery (SPAIR) sequences, executed in both axial and sagittal planes, with a series of six repetitions at one-minute intervals post-contrast injection.

The imaging parameters were meticulously set for each sequence. For TSE T1A: Repetition Time (TR) 476 ms, Echo Time (TE) 11 ms, matrix 384x297, Number of Excitations (NEX) 1, slice thickness 4 mm. TIRM T2A parameters included TR 2250 ms, TE 56 ms, Inversion Time (TI) 165 ms, matrix 384x270, NEX 1, slice thickness 4 mm. Axial T2A TSE sequences were characterized by TR 5350 ms, TE 76 ms, matrix 320x217, NEX 2, slice thickness 4 mm. The dynamic sequences featured TR 4.53 ms, TE 1.82 ms, flip angle 10°, matrix 416x313, NEX 1, slice thickness 2 mm. Additionally, diffusion-weighted imaging (DWI) was performed using the echo-planar imaging (EPI) technique with diffusion-sensitive gradients in three orthogonal directions (x, y, z), utilizing b-values of 50, 200, and 800 s/mm². Diffusion parameters were set to TR 6400 ms, TE 66 ms, matrix 220x84, NEX 2, with a slice thickness of 4 mm.

2.4. Radiologist Evaluation and Lesion Characterization

Two radiologists evaluated all MR images. The assessed features included:

1. Breast Composition: Classified according to the BI-RADS system [31].

2. Background Contrast Enhancement: Non-pathological enhancement of fibroglandular tissue, categorized into four levels: Minimal (<25%), Light (25-50%), Medium (50-75%), and Distinctive (>75%).

3. Lesion Characteristics:

- Location: Upper outer quadrant, upper inner quadrant, retroareolar, lower outer quadrant, lower inner quadrant.
- Volume: Determined by volume measurement.
- Shape: Round, oval, irregular.
- Edge: Sharp, veiled, microlobulated, indistinct, spiculated.
- T1 Signal: Isointense, hypointense, hyperintense relative to parenchyma.
- T2 Signal: Isointense, hypointense, hyperintense relative to parenchyma.
- Contrast Enhancement Pattern: Homogeneous, contrast enhancing septa, heterogeneous, none, peripheral.
- Diffusion Property: Compared to parenchyma (less, equal, more).
- Contrast Enhancement Curve: Type 1, 2, or 3.
- ADC Value: Recorded.

4. Other Lesions: Presence of multifocality and multicentricity.

2.5. Radiomics-based Texture Analysis

MRI data of the enrolled cases, encompassing sequences, including T1A, T2A, early and late-phase post-contrast T1A, and diffusion-weighted imaging, were acquired in Digital Imaging and Communications in Medicine (DICOM) format. These images were then processed using the MaZda 4.6 software, a specialized tool for texture analysis developed by Szczypinski et al. [32]. A critical step involved the demarcation of the mass on the images by defining a Region of Interest (ROI). Recognizing the impact of ROI size on texture analysis outcomes, as evidenced in previous

studies [33], a uniform ROI of 10x10 pixels was employed for each lesion. Adhering to established protocols, the ROI was strategically placed on the most solid and contrast-enhanced segment of the lesion (Figure 1) [34].

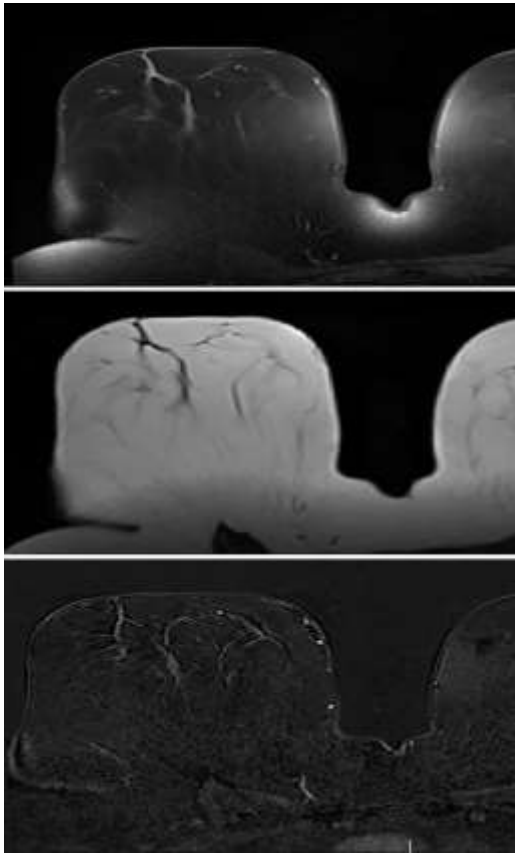

Figure 1: Region-of-interest (ROI) placement for texture analysis on T1A, T2A and postcontrast T1A subtraction images of the same patient.

The MaZda software facilitated a multifaceted texture analysis, starting with a histogram analysis that provides a global assessment based on pixel intensity, independent of spatial pixel relationships. The gradient analysis was executed by computing the gradient histogram of image intensity distribution. Co-occurrence Matrix (COM) analysis was employed to evaluate spatial relations and densities of pixel pairs at varied angles. Additionally, Run-Length Matrix (RLM) analysis was conducted to assess pixel runs of specific gray scale levels and lengths across four orientations (horizontal, vertical, 45°, and 135°). This comprehensive analysis by the software yielded a detailed report for each case, summarizing diverse texture features. Considering the anticipated homogeneity across four-directional analyses, these values were consolidated into a singular parameter [35]. Hereafter, three-dimensional texture analysis was executed on the MR images in DICOM format using the MaZda 4.6 software. This analysis yielded several histogram-based features, including mean brightness, variance, skewness, and kurtosis. Additionally, 11 features were extracted from the gray-level co-occurrence matrix as part of the Second Order Texture Analysis. These features included Angular Second Moment (AngScMom), Contrast, Correlation (Correlat), Sum of Squares (SumofSqs), Inverse Difference Moment (InvDfMom), Sum Average (SumAverg), Sum Variance (SumVarnc), Sum Entropy (SumEntrp), Entropy, Difference Variance (DifVarnc), and Difference Entropy (DifEntrp).

2.6. Machine Learning

We explored the predictive power of various machine learning models for classification tasks (molecular characteristics prediction [luminal A, luminal B, Her2, Triple negative], p53 expression prediction, lymphovascular invasion, and lymph node metastasis) using a comprehensive dataset incorporating clinical, anatomical, and radiomics features. The dataset was meticulously curated to include a range of

variables, from basic clinical information to advanced radiomics markers derived from T1-weighted, T2-weighted, early, and late post-contrast T1, and DWI sequences.

The data preprocessing pipeline was established to accommodate both categorical and numerical variables, ensuring the compatibility of data types for machine learning algorithms. Categorical variables were encoded using one-hot encoding to transform them into a machine-readable format. This encoding facilitates the handling of non-ordinal categorical data without imposing any ordinal relationship, which could mislead the learning process. Numerical variables and a wide array of radiomics features quantifying tumor heterogeneity and texture, were standardized to have a mean of zero and a standard deviation of one. This standardization is crucial for models sensitive to the scale of the data, ensuring that all features contribute equally to the model's prediction capability. A stratified k-fold cross-validation method was adopted, with five folds, to evaluate the models' performance and ensure that each fold was a good representative of the whole. Four machine learning models were assessed: Logistic Regression, Random Forest, Gradient Boosting, and XGBoost. Each model was evaluated on its ability to accurately classify the target variables categories based on the comprehensive feature set. Performance metrics such as accuracy, precision, recall, F1 score, and the Area Under the Receiver Operating Characteristic Curve (AUC-ROC) were calculated for each fold and averaged to gauge the models' overall efficacy. To further understand the models' decision-making processes, a feature importance analysis was conducted using the Random Forest classifier. This analysis highlights the most influential features driving the classification, providing insights into the biological and clinical significance of various predictors. The top ten features were visualized to demonstrate their relative importance in the model's predictive performance. All machine learning analyses, and preprocessing steps were conducted using Python.

2.7. Statistical Analyses

Statistical analyses were performed using the SPSS 22 demo package program. Descriptive analyses in the study presented numerical variables as mean, median, standard deviation, minimum-maximum values, and categorical variables as counts, ratios, and percentages. The normal distribution of the data was tested using the Shapiro-Wilk test. For intergroup comparisons, appropriate analytical tests, such as Kruskal-Wallis (including Dunn's post hoc test), independent t-test, One-Way-ANOVA (including Tukey HSD test) and Mann-Whitney U tests (Bonferroni adjusted) were utilized according to the nature of the variables. P-values less than 0.05 were considered statistically significant.

Results

3.1. Descriptive statistics

This study encompassed a total of 70 cases, with the ages of participants ranging from 28 to 86 years. The average age was determined to be 55.19 years, with a standard deviation of 13.31 years, reflecting a broad age distribution among the study population. The lesion volumes exhibited considerable variation, ranging from 429 mm^3 to 125,896 mm^3, and had an average volume of 11,504 mm^3.

Upon examining the histopathological and molecular characteristics, we found a diverse representation of tumor subtypes. Luminal A tumors accounted for 18.6% of the cases

(n=13), Luminal B for 38.6% (n=27), HER2-overexpressed for 12.9% (n=9), and triple-negative for 30.0% (n=21). This distribution underscores the molecular heterogeneity within the cohort. The grading of tumors revealed a near-equitable split, with 45.7% (n=32) classified as low-grade and 54.3% (n=38) as high-grade, paralleling the distribution of the Ki-67 proliferation index, where 45.7% exhibited low (ki-67-) and 54.3% high (ki-67+) expression levels.

Additional molecular markers provided further insights into tumor characteristics. The p53 protein showed negative expression in 61.4% of cases (n=43), medium positive in 17.1% (n=12), and strong positive in 21.4% (n=15). The Cerb-B2 (HER2) status was negative in 77.1% of cases (n=54) and positive in 22.9% (n=16). Estrogen receptor (ER) status was positive in 57.1% of cases (n=40) and negative in 42.9% (n=30), while progesterone receptor (PR) status was similarly distributed, with 51.4% positive (n=36) and 48.6% negative (n=34). Lymphovascular invasion was observed in 41.4% of cases (n=29), and lymph node metastasis was present in 51.4% of the cohort (n=36), reflecting the aggressive nature of some tumors. The response to neoadjuvant therapy was evaluated in 30.0% of cases (n=21), with 47.6% (n=10) showing a positive response and 52.4% (n=11) showing no response, indicating a varied therapeutic efficacy. The majority of patients did not receive neoadjuvant therapy (n=49, 70.0%).

Breast MRI evaluations revealed that the most common breast composition was type B, observed in 45.7% of cases (n=32), followed by type C in 28.6% (n=20), type D in 14.3% (n=10), and type A in 11.4% (n=8). Lesion localization predominantly occurred in the upper outer quadrant (57.1%, n=40), with multifocality and multicentricity rates noted at 28.6% (n=20) and 14.3% (n=10), respectively. All lesions exhibited more diffusion restriction than the surrounding parenchyma, and 84.3% (n=59) demonstrated a heterogeneous contrast pattern with rapid early enhancement in 88.6% of cases (n=62).

Lesion characteristics further included a majority with an irregular shape (85.7%, n=60), and the edges of the lesions were most often microlobulated (51.4%, n=36) or spiculated (42.9%, n=30). Satellite nodules were present in 42.9% of the cases (n=30). When considering the T1 and T2 signal characteristics, the lesions were predominantly isointense on T1 (64.3%, n=45) and exhibited a mix of signal intensities on T2, with 51.4% isointense (n=36), 31.4% hyperintense (n=22), and 17.1% hypointense (n=12). The contrast enhancement patterns were primarily heterogeneous (84.3%, n=59) or showed peripheral enhancement (10%, n=7), with rapid enhancement being the most common dynamic feature (88.6%, n=62).

		Mean	Std	Count	%
Age		55.19	13.31		
Lesion Volume		1.15	0.21		
Molecular characteristics	Luminial A			13	18.6%
	Luminal B			27	38.6%
	Her2 overexpressed			9	12.9%
	Triple (-)			21	30.0%
Grade	low			32	45.7%
	high			38	54.3%
Ki-67	ki-67-			32	45.7%
	ki-67+			38	54.3%
p53	negative			43	61.4%

	medium positive			12	17.1%
	strong positive			15	21.4%
cerb-2	Cerb-B2-			54	77.1%
	Cerb-B2+			16	22.9%
ER	ER-			30	42.9%
	ER+			40	57.1%
PR	PR-			34	48.6%
	PR+			36	51.4%
Lymphovascular Invasion	no			41	58.6%
	yes			29	41.4%
Lymph Node Metastasis	no			34	48.6%
	yes			36	51.4%
Neoadjuvant response	no			11	52.4%
	yes			10	47.6%
	No neoadjuvant therapy			49	70.0%
Breast Pattern	A			8	11.4%
	B			32	45.7%
	C			20	28.6%
	D			10	14.3%
Background Contrast Enhancement	1			32	45.7%
	2			19	27.1%
	3			17	24.3%
	4			2	2.9%
Lesion Location	Upper outer quadrant			40	57.1%
	Upper inner quadrant			16	22.9%
	Lower outer quadrant			8	11.4%
	Lower inner quadrant			3	4.3%
	Retro			3	4.3%
BIRADS	4A			0	0.0%
	4B			0	0.0%
	4C			22	31.4%
	5			48	68.6%
Shape	round			9	12.9%
	oval			1	1.4%
	irregular			60	85.7%
Edge	sharp			3	4.3%
	veiled			0	0.0%
	microlobulated			36	51.4%
	indistinct			1	1.4%
	spiculated			30	42.9%
Satellite	no			40	57.1%
	yes			30	42.9%
Multifocal	no			50	71.4%
	yes			20	28.6%
Multicentric	no			60	85.7%
	yes			10	14.3%
T1 Signal	iso			45	64.3%
	hypo			1	1.4%
	hyper			24	34.3%
T2 Signal	iso			36	51.4%
	hypo			12	17.1%
	hyper			22	31.4%

Diffusion restriction	less than parenchyma			0	0.0%
	equal to parenchyma			0	0.0%
	more than parenchyma			70	100.0%
Contrast pattern	homogeneous			4	5.7%
	contrast enhancing septa			0	0.0%
	heterogeneous			59	84.3%
	no contrast enhancement			0	0.0%
	peripheral contrast enhancement			7	10.0%
Contrast enhancement	slow			5	7.1%
	medium			3	4.3%
	rapid			62	88.6%
Contrast enhancement curve	type 1			4	5.7%
	type 2			50	71.4%
	type 3			16	22.9%

Table 2: Demographic, anatomical and molecular characteristics of the cohort.

3.2. Pairwise analyses of radiomics features

Significant findings emerged across various target variables when comparing different aspects of the radiomics feature set. The visualization of radiomics feature set expression among the target variables can be found in the form of heatmaps in the supplementary figure material (supplementary figures 1-5). These findings were derived from statistical tests applied to assess the association of specific radiomics features with outcomes, including neoadjuvant response, molecular characteristics, p53 status, lymphovascular invasion, lymph node metastasis, and neoadjuvant response at different times (T1, T2, earlyT1, lateT1, DWI). For the target variable of neoadjuvant response using T1 modality, several features were significantly associated with the response. Variance of T1 signal (Variance_T1SignalA), Angular Second Moment (AngularSecondMoment_T1SignalA), Contrast (Contrast_T1SignalA), Sum of Squares (SumofSquares_T1SignalA), Inverse Difference Moment (InverseDifferenceMoment_T1SignalA), Sum Variance (SumVariance_T1SignalA), Sum Entropy (SumEntropy_T1SignalA), and Entropy (Entropy_T1SignalA) all showed significant differences between patients who did and did not respond to neoadjuvant therapy, with p-values ranging from 0.0067 to 0.0486. In the context of molecular characteristics at T2, the mean T2 signal (Mean_T2SignalA) showed a significant difference between Luminal A and Triple Negative cases, with a p-value of 0.0329. Similarly, early T1 variance (Variance_earlyT1SignalA) differed significantly between Luminal A and Luminal B, indicating potential as a distinguishing feature.

Regarding the p53 status, Skewness of the early T1 signal (Skewness_earlyT1SignalA) was notably different between cases with negative and strong positive p53 expression, with a p-value of 0.0291. Lymphovascular invasion also correlated with differences in early T1 Difference Entropy (DifferenceEntropy_earlyT1SignalA), suggesting its potential use in assessing invasion status. In late T1, features such as Mean, Inverse Difference Moment, Sum Average, and Difference Entropy

(Mean_lateT1Signala, InverseDifferenceMoment_lateT1Signala,SumAverage_lateT1Signala,DifferenceEntropy_lateT1Signala) were significantly associated with neoadjuvant response, indicating that changes in these parameters could reflect response to therapy. The DWI signal offered several significant associations. For instance, the mean DWI signal (Mean_DWI) was significantly different between Luminal A and Triple Negative categories, and various features, including Contrast, Inverse Difference Moment, and Difference Variance (Contrast_DWI, InverseDifferenceMoment_DWI, DifferenceVariance_DWI), revealed significant differences across different levels of p53 expression. Particularly, the Inverse Difference Moment showed a significant difference between medium and strong positive p53 expression, with a p-value of 0.0012. Lymph node metastasis showed significant associations with DWI features such as Skewness, Correlation, and Entropy (Skewness_DWI, Correlation_DWI, Entropy_DWI), with p-values indicating these features could be important markers of metastatic involvement. Lastly, the DWI signal also related significantly to neoadjuvant response, with Mean, Skewness, Contrast, Difference Variance, and Difference Entropy (Mean_DWI, Skewness_DWI, Contrast_DWI, DifferenceVariance_DWI, DifferenceEntropy_DWI) demonstrating significant differences between responders and non-responders, providing a radiomic signature of treatment efficacy.

In the next step, we assessed the predictive value of machine learning models to predict the target variables. We did not assess neoadjuvant treatment response with the machine learning models, as the number of patients receiving neoadjuvant treatment was too small for reliable prediction modelling using these models.

3.4. Prediction of molecular characteristics (Luminal A, Luminal B, Her2, Triple-Negative) with radiomics feature set

For the prediction of T1 molecular characteristics, which include Luminal A, Luminal B, Her2, and Triple-Negative classes, four machine learning models were evaluated: Logistic Regression, Random Forest, Gradient Boosting, and XGBoost. The models were assessed based on their mean accuracy, area under the curve (AUC), F1 score, precision, and recall, with a feature set that combined radiomic, clinical, and anatomical features. The results revealed a generally low predictive capability. XGBoost outperformed other models, showing the highest mean accuracy of 45.71% and a mean AUC of 67.11%, indicating a better overall performance in distinguishing between the different molecular characteristics. The F1 score for XGBoost was also the highest at 43.26%, which is a harmonic mean of precision and recall, suggesting a balanced classification performance. XGBoost's precision and recall were the highest amongst the models, with values of 44.84% and 45.71%, respectively, suggesting a consistent ability to correctly identify the positive classes while maintaining a lower rate of false positives. In contrast, Logistic Regression and Gradient Boosting exhibited identical mean accuracies and mean recalls of 41.43%. However, Logistic Regression demonstrated a slightly higher mean AUC (64.54%) compared to Gradient Boosting (62.56%). Logistic Regression also had a marginally higher mean F1 score and precision of 40.51% and 42.59%, respectively, compared to those of Gradient Boosting. Random Forest, while not leading in any particular metric for T1 prediction, did display a competitive mean AUC of 68.01%, the

highest among the models, suggesting its strength in the probabilistic separation of classes.

3.5. Prediction of p53 status with radiomics feature set

The predictive performance of four machine learning models—Logistic Regression, Random Forest, Gradient Boosting, and XGBoost—was compared to determine the p53 status, utilizing a composite feature set encompassing radiomic, clinical, and anatomical data. Random Forest demonstrated superior mean accuracy (64.29%) and mean recall (64.29%) for T1 prediction, indicating its robustness in correctly identifying the p53 positive cases. Its performance was also notable in the AUC with a mean score of 64.10%, suggesting a moderate trade-off between true positive rate and false positive rate compared to other models. Logistic Regression, while having a lower mean accuracy for T1 (61.43%), showed a competitive mean AUC of 53.93%. The model maintained a commendable balance between precision and recall, indicated by a mean F1 score of 57.00% and the highest mean recall of 61.43%, emphasizing its potential utility in scenarios where minimizing false negatives is critical. Gradient Boosting and XGBoost exhibited varied performance across different metrics. For early T1 prediction, Gradient Boosting outperformed all other models with the highest mean accuracy (64.29%) and mean AUC (69.67%), suggesting its efficacy in p53 status prediction using early T1. XGBoost, despite lower scores in some metrics, showed a respectable mean AUC of 62.39% for T1 prediction and a balanced mean F1 score of 56.22% for T1 late prediction, indicating its capability as a competitive alternative. For T2, Logistic Regression and Random Forest presented closely matched mean accuracies of 58.57% and 60.00%, respectively, with Random Forest slightly leading in mean AUC. This suggests that Random Forest might be slightly more effective for T2 prediction, especially when considering its higher mean recall, which could be crucial in clinical decision-making. In the case of DWI prediction, Logistic Regression and XGBoost shared the highest mean accuracy (61.43%), while Logistic Regression also exhibited a strong mean AUC (63.46%), underscoring its potential as a reliable predictive tool for p53 status in DWI scenarios. Overall, Random Forest and Gradient Boosting demonstrated strong performance in accuracy and AUC for T1 and T1 early prediction, respectively. Logistic Regression showed promise in terms of recall across the board, which might make it preferable in clinical settings where the cost of missing a positive case is high.

3.6. Prediction of lymph node invasion with radiomics feature set

In the next step we compared the performance of the predictive models in determining the likelihood of lymph node invasion using a combined set of radiomic, clinical, and anatomical features. Overall, the predictive capability was low to moderate. XGBoost emerged as the leading model, particularly for T1 and DWI prediction, with the highest mean accuracy (58.93% for T1 and 64.29% for DWI) and mean recall (58.93% for T1 and 64.29% for DWI). This suggests XGBoost's superior capability to correctly identify cases with lymph node invasion compared to the other models. Furthermore, its mean AUC of 54.69% for T1 and 62.50% for DWI indicates a moderate ability to discriminate between positive and negative cases. For late T1 prediction, Random Forest was the standout model, achieving the highest mean accuracy (67.86%) and an impressive mean recall of 67.86%. These results

underscore the model's predictive strength, particularly in lymph node invasion detection using the late T1 modality. Random Forest also achieved the highest mean AUC (57.29%) for late T1, further demonstrating its effectiveness in this context. Gradient Boosting showed notable performance in the early T1 modality, with the highest mean accuracy (60.71%) and the highest mean AUC (62.50%), indicating its potential as an predictor of lymph node invasion. It also maintained a competitive mean F1 score across early T1 (59.02%) and late T1 (58.10%) stages, reflecting a balanced precision and recall. Logistic Regression, despite showing the lowest performance in terms of mean accuracy and mean AUC across all stages, provided a consistent recall rate, which could be valuable in clinical scenarios where identifying all positive cases is critical, even at the expense of increased false positives. The F1 scores, reflecting the balance between precision and recall, were generally highest for XGBoost and Random Forest, with XGBoost leading in T1 and DWI, and Random Forest in T1 late. This suggests that these models are better at maintaining a balance between the precision and recall, which is often crucial in a clinical setting. In summary, the analysis indicates XGBoost as the most consistent model for lymph node invasion prediction across different modalities, with Random Forest as a potential alternative, especially in the T1 late modality.

3.7. Prediction of lymph node metastasis with radiomics feature set

Further, we assessed lymph node metastasis prediction with the four machine learning models, using a dataset that incorporated radiomics features along with clinical and anatomical characteristics. The results indicated a moderate capability of prediction. Gradient Boosting showed exceptional performance, particularly in predicting T1 and DWI metastasis, with the highest mean accuracy of 67.86% and 62.50%, respectively. Its ability to discriminate between cases was also highlighted by the highest mean AUC of 70.04% for T1 and 64.44% for DWI. Moreover, Gradient Boosting achieved the highest mean F1 score of 67.86% for T1 and 62.50% for DWI, indicating a strong balance between precision and recall, which is crucial for the reliable identification of metastatic lymph nodes. Logistic Regression and XGBoost both demonstrated a mean accuracy of 62.50% for T1, with XGBoost matching Logistic Regression's mean recall of 67.21%. These models performed equally well in early T1 prediction, each with a mean accuracy of 62.50%, although XGBoost exhibited a slightly higher mean AUC. Random Forest, while not leading in mean accuracy, did show robust performance with a higher mean recall, especially for T2 (66.60%), suggesting its potential utility in scenarios where identifying as many positive cases as possible is a priority. The metrics indicate that while Gradient Boosting stands out for its overall performance in T1 and DWI prediction, XGBoost and Logistic Regression may offer advantages in early-stage lymph node metastasis detection due to their higher recall rates. However, for late T1 prediction, Gradient Boosting again takes the lead with the highest mean accuracy (64.29%) and mean recall (73.91%).

Discussion

The principal aim of this study was to meticulously explore the association between MRI texture characteristics of confirmed malignant breast masses and their corresponding histopathological and molecular features, alongside their response to

neoadjuvant treatments. Our comprehensive analysis revealed significant associations between MRI-derived texture features and intratumoral heterogeneity, reflecting in the variations of histopathological grading and molecular subtyping. Although our results revealed moderate predictive capability, these findings substantiate the hypothesis that MRI texture analysis holds valuable predictive power in assessing pathological outcomes and responses to neoadjuvant therapy. The implications of these results are profound, offering a promising avenue for enhancing personalized treatment strategies in breast cancer management.

The use of radiomics in breast imaging is making significant progress in differentiating between harmful and non/less-harmful lesions, identifying tumor characteristics, and predicting the effectiveness of treatments and the likelihood of cancer returning [27,36,37]. Our research focused on further exploring these relationships, specifically looking at how MRI texture features can reveal the complexity within a tumor. This method shows potential in improving the accuracy of predicting disease outcomes and customizing treatment plans for breast cancer patients [13,38]. While radiomics and its combination with genomics hold great promise for creating more personalized medicine approaches, their full potential is yet to be realized. Key challenges include the need for independently verified data to prove their value in diagnosis and prognosis, the ongoing development towards practical clinical use, and overcoming obstacles such as incomplete patient data, fragmented data integration, and misunderstandings about data privacy and sharing [39–41]. Early detection and detailed analysis of breast cancer are critical for improving patient survival rates, particularly for those with early-stage, localized disease that can be cured [24,42]. Current methods for diagnosing breast cancer involve a combination of radiology, clinical examination, and tissue analysis, each with its own drawbacks, such as limited sensitivity, invasiveness, and the possibility of missing important lesion characteristics, which could lead to additional biopsies.

Radiomics offers a new horizon in diagnostics by extracting unique, quantitative data from breast cancer imaging, potentially reducing the need for invasive biopsy procedures and enabling more personalized patient care. Our findings align with previous research, such as the work of Zhou et al. [43] and Xie et al. [44], who demonstrated the ability of DCE-MRI texture analysis to accurately distinguish between benign and malignant breast lesions. These advancements are crucial for improving the precision and reliability of breast cancer diagnosis. Further studies, including those by Li et al. [45] and an analysis of DWI-based radiomics [46], affirm radiomics' role in enhancing diagnostic accuracy, minimizing false positives, and augmenting traditional mammography. The adaptability of radiomics across different imaging techniques, such as demonstrated in tomosynthesis and ultrasound applications by Tagliafico et al. [47] and Luo et al. [48], showcases its versatility. In predicting molecular subtypes and treatment responses, research by Fan et al. [49], Xie et al. [50], and Demircioglu et al. [51] has shown that DCE-MRI-based radiomic features, when combined with clinical data, strongly correlate with breast cancer's molecular characteristics. This collective evidence supports the non-invasive characterization of breast tumors using radiomics.

Pre-surgery chemotherapy is becoming more common in the management of operable breast cancer, known for its benefits in

treatment response and reducing the chance of cancer returning [24]. Predicting complete response to treatment before surgery remains a challenge, typically assessed after the surgical removal of tumors [89,90]. Our study, along with others [6,19,29,49,52–55], suggests that MRI radiomic features can predict complete treatment response, indicating a move towards non-invasive treatment monitoring. Insights from Choudhery et al. [55] and Braman et al. [54], along with earlier research [19,49,56,57], highlight the importance of analyzing DCE-MRI radiomic features before treatment to predict complete response to chemotherapy, suggesting these features could be important markers in breast cancer therapy. Our research adds to this by identifying a radiomic score that predicts response to chemotherapy, incorporating clinical and biological data to enhance predictions of treatment outcomes before they begin. With further validation, this could transform treatment planning by identifying patients less likely to benefit from certain therapies, avoiding unnecessary treatments.

The status of axillary lymph nodes is crucial for determining breast cancer prognosis [58,59]. Radiomics has shown potential in predicting lymph node involvement, with studies creating predictive models that combine radiomic and clinical-pathological data for more accurate patient classification [60–62]. These models have proven effective across various imaging methods, indicating high diagnostic accuracy [60–62]. However, the broad applicability of radiomics across different patient populations and imaging settings remains a challenge. Research by Cattell et al. [63] comparing deep learning features with traditional radiomics highlights the potential for greater model adaptability with deep learning, especially in handling various imaging resolutions. This underscores the evolving synergy between machine learning and deep learning in radiomics, where combining approaches could lead to stronger predictive models.

The risk of breast cancer recurrence is a major concern, with radiomics offering new avenues for predicting this risk. This could significantly change treatment strategies, ensuring patients at low risk avoid unnecessary treatments while those at high risk receive adequate intervention [64]. Recent studies using breast MRI have linked radiomic features from pre-treatment DCE-MRI with recurrence risk in invasive breast cancer [65–67]. For instance, Park et al. [65] and Mazurowski et al. [67] identified radiomic signatures associated with different survival outcomes. Our research builds on these findings, showing that combining MRI radiomic features with data from normal breast tissue can improve predictions of recurrence risk, suggesting the broader breast environment plays a critical role in recurrence, potentially even more so than the tumor itself.

While MRI provides a broad set of imaging features for prediction modelling, advances in ultrasound radiomics, as seen in the work of Xiong et al. [68] and Yu et al. [69], have also led to the development of models for predicting disease-free survival in invasive breast cancer, enhancing clinical decision-making. Additionally, Dasgupta et al. [70] demonstrated the predictive power of quantitative ultrasound radiomics in identifying patients at risk of recurrence, achieving an accuracy of 82%. In mammography, the model developed by Mao et al. [71] incorporating radiomic features shows significant promise in breast cancer risk prediction, reinforcing the potential of integrating radiomics into regular imaging practices to enhance prognostic capabilities. In

summary, while integrating radiomic features into clinical practice offers exciting possibilities, there are complexities in achieving routine clinical adoption. Steps such as ensuring consistent results across various datasets, standardizing the process of feature extraction, and harmonizing imaging protocols are vital. Addressing these challenges is key to enabling radiomics to refine and personalize breast cancer management further.

Our study brings to light both strengths and limitations. We carefully selected our participants using well-defined criteria, ensuring our study group was both relevant and consistent. The collaboration with the Department of Pathology enriched our analysis with a diverse range of data, including morphological, molecular, and radiomic insights. By employing a 1.5 Tesla MRI system, we captured high-quality images that revealed intricate texture details, enabling a thorough analysis. Our adherence to the established Bloom-Richardson grading system and a uniform approach to immunohistochemical staining ensured the reliability of our histopathological data for comparison with MRI features. The use of MaZda 4.6 software for texture analysis provided us with detailed radiomic data, and the application of sophisticated machine learning models allowed us to investigate the potential of these features in identifying different clinical and molecular aspects of breast cancer. Our study's statistical rigor, supported by a selection of tests appropriate for our data, lent credibility to our conclusions. However, the study's relatively short duration limited our ability to gather long-term data and observe extended outcomes.

On the downside, the study's sample size of 70 cases, while adequate for initial exploration, may fall short of providing a basis for broader generalizations. Being a retrospective study, it is naturally prone to biases typical of such research designs, including selection bias and potential impacts from factors not measured in the study. The research being conducted in a single institution could mean the findings are specific to that environment, potentially limiting their broader applicability. The absence of prospective validation leaves questions about the real-world effectiveness of our predictive models. The fact that only some participants underwent neoadjuvant treatment may affect the universality of those specific findings. Our reliance on data from post-surgery histopathology restricts the use of radiomic features for making real-time, pre-surgical decisions. Despite a consistent MRI protocol, individual differences in patient physiology and timing of scans could introduce variability in the imaging results. External validation, particularly in multi-center studies, is essential to confirm the reproducibility and reliability of our findings.

Conclusion

In summary, while our study enriches the understanding of how MRI radiomics features correlate with breast cancer characteristics, further research is needed to truly establish these findings' clinical utility. Expanding the scope to include larger, more diverse cohorts and employing prospective study designs will be crucial for moving beyond the preliminary insights provided here.

WORKS CITED

1. Sung, H.; Ferlay, J.; Siegel, R.L.; Laversanne, M.; Soerjomataram, I.; Jemal, A.; Bray, F. Global Cancer Statistics 2020: GLOBOCAN Estimates of Incidence and Mortality Worldwide for 36 Cancers in 185 Countries. CA. Cancer J. Clin. 2021, 71, 209–249, doi:10.3322/caac.21660.
2. Arnold, M.; Morgan, E.; Rumgay, H.; Mafra, A.; Singh, D.; Laversanne, M.; Vignat, J.; Gralow, J.R.; Cardoso, F.; Siesling, S.; et al. Current and Future Burden of Breast Cancer: Global Statistics for 2020 and 2040. Breast Edinb. Scotl. 2022, 66, 15–23, doi:10.1016/j.breast.2022.08.010.
3. World Health Organization WHO Position Paper on Mammography Screening; World Health Organization: Geneva, 2014; ISBN 978-92-4-150793-6.
4. Mann, R.M.; Kuhl, C.K.; Moy, L. Contrast-enhanced MRI for Breast Cancer Screening. J. Magn. Reson. Imaging 2019, 50, 377–390, doi:10.1002/jmri.26654.
5. Xiao, J.; Rahbar, H.; Hippe, D.S.; Rendi, M.H.; Parker, E.U.; Shekar, N.; Hirano, M.; Cheung, K.J.; Partridge, S.C. Dynamic Contrast-Enhanced Breast MRI Features Correlate with Invasive Breast Cancer Angiogenesis. Npj Breast Cancer 2021, 7, 42, doi:10.1038/s41523-021-00247-3.
6. Teruel, J.R.; Heldahl, M.G.; Goa, P.E.; Pickles, M.; Lundgren, S.; Bathen, T.F.; Gibbs, P. Dynamic Contrast-Enhanced MRI Texture Analysis for Pretreatment Prediction of Clinical and Pathological Response to Neoadjuvant Chemotherapy in Patients with Locally Advanced Breast Cancer. NMR Biomed. 2014, 27, 887–896, doi:10.1002/nbm.3132.
7. Cao, K.; Zhao, B.; Li, X.-T.; Li, Y.-L.; Sun, Y.-S. Texture Analysis of Dynamic Contrast-Enhanced MRI in Evaluating Pathologic Complete Response (pCR) of Mass-Like Breast Cancer after Neoadjuvant Therapy. J. Oncol. 2019, 2019, 4731532, doi:10.1155/2019/4731532.
8. Gillies, R.J.; Kinahan, P.E.; Hricak, H. Radiomics: Images Are More than Pictures, They Are Data. Radiology 2016, 278, 563–577, doi:10.1148/radiol.2015151169.
9. Aerts, H.J.W.L.; Velazquez, E.R.; Leijenaar, R.T.H.; Parmar, C.; Grossmann, P.; Carvalho, S.; Bussink, J.; Monshouwer, R.; Haibe-Kains, B.; Rietveld, D.; et al. Decoding Tumour Phenotype by Noninvasive Imaging Using a Quantitative Radiomics Approach. Nat. Commun. 2014, 5, 4006, doi:10.1038/ncomms5006.
10. Davnall, F.; Yip, C.S.P.; Ljungqvist, G.; Selmi, M.; Ng, F.; Sanghera, B.; Ganeshan, B.; Miles, K.A.; Cook, G.J.; Goh, V. Assessment of Tumor Heterogeneity: An Emerging Imaging Tool for Clinical Practice? Insights Imaging 2012, 3, 573–589, doi:10.1007/s13244-012-0196-6.
11. Grossmann, P.; Stringfield, O.; El-Hachem, N.; Bui, M.M.; Rios Velazquez, E.; Parmar, C.; Leijenaar, R.T.; Haibe-Kains, B.; Lambin, P.; Gillies, R.J.; et al. Defining the Biological Basis of Radiomic Phenotypes in Lung Cancer. eLife 2017, 6, e23421, doi:10.7554/eLife.23421.
12. Ibrahim, A.; Vallieres, M.; Woodruff, H.; Primakov, S.; Beheshti, M.; Keek, S.; Sanduleanu, S.; Walsh, S.; Morin, O.; Lambin, P. Radiomics Analysis for Clinical Decision Support in Nuclear Medicine. In Proceedings of the Seminars in nuclear medicine; Elsevier, 2019; Vol. 49, pp. 438–449.
13. Lambin, P.; Leijenaar, R.T.H.; Deist, T.M.; Peerlings, J.; de Jong, E.E.C.; van Timmeren, J.; Sanduleanu, S.; Larue, R.T.H.M.; Even, A.J.G.; Jochems, A.; et al. Radiomics: The Bridge between Medical Imaging and Personalized Medicine. Nat. Rev. Clin. Oncol. 2017, 14, 749–762, doi:10.1038/nrclinonc.2017.141.
14. Walsh, S.; de Jong, E.E.C.; van Timmeren, J.E.; Ibrahim, A.; Compter, I.; Peerlings, J.; Sanduleanu, S.; Refaee, T.; Keek, S.; Larue, R.T.H.M.; et al. Decision Support Systems in Oncology. JCO Clin. Cancer Inform. 2019, 3, 1–9, doi:10.1200/CCI.18.00001.
15. Milenković, J.; Dalmış, M.U.; Žgajnar, J.; Platel, B. Textural Analysis of Early-Phase Spatiotemporal Changes in Contrast Enhancement of Breast Lesions Imaged with an Ultrafast DCE-MRI Protocol. Med. Phys. 2017, 44, 4652–4664, doi:10.1002/mp.12408.
16. Parekh, V.S.; Jacobs, M.A. Integrated Radiomic Framework for Breast Cancer and Tumor Biology Using Advanced Machine Learning and Multiparametric MRI. NPJ Breast Cancer 2017, 3, 43, doi:10.1038/s41523-017-0045-3.
17. Liu, Z.; Li, Z.; Qu, J.; Zhang, R.; Zhou, X.; Li, L.; Sun, K.; Tang, Z.; Jiang, H.; Li, H.; et al. Radiomics of Multiparametric MRI for Pretreatment Prediction of Pathologic Complete Response to Neoadjuvant Chemotherapy in Breast Cancer: A Multicenter Study. Clin. Cancer Res. Off. J. Am. Assoc. Cancer Res. 2019, 25, 3538–3547, doi:10.1158/1078-0432.CCR-18-3190.
18. Xiong, Q.; Zhou, X.; Liu, Z.; Lei, C.; Yang, C.; Yang, M.; Zhang, L.; Zhu, T.; Zhuang, X.; Liang, C.; et al. Multiparametric MRI-Based Radiomics Analysis for Prediction of Breast Cancers Insensitive to

Neoadjuvant Chemotherapy. Clin. Transl. Oncol. Off. Publ. Fed. Span. Oncol. Soc. Natl. Cancer Inst. Mex. 2020, 22, 50–59, doi:10.1007/s12094-019-02109-8.
19. Cain, E.H.; Saha, A.; Harowicz, M.R.; Marks, J.R.; Marcom, P.K.; Mazurowski, M.A. Multivariate Machine Learning Models for Prediction of Pathologic Response to Neoadjuvant Therapy in Breast Cancer Using MRI Features: A Study Using an Independent Validation Set. Breast Cancer Res. Treat. 2019, 173, 455–463, doi:10.1007/s10549-018-4990-9.
20. Waugh, S.A.; Purdie, C.A.; Jordan, L.B.; Vinnicombe, S.; Lerski, R.A.; Martin, P.; Thompson, A.M. Magnetic Resonance Imaging Texture Analysis Classification of Primary Breast Cancer. Eur. Radiol. 2016, 26, 322–330, doi:10.1007/s00330-015-3845-6.
21. Monti, S.; Aiello, M.; Incoronato, M.; Grimaldi, A.M.; Moscarino, M.; Mirabelli, P.; Ferbo, U.; Cavaliere, C.; Salvatore, M. DCE-MRI Pharmacokinetic-Based Phenotyping of Invasive Ductal Carcinoma: A Radiomic Study for Prediction of Histological Outcomes. Contrast Media Mol. Imaging 2018, 2018, 5076269, doi:10.1155/2018/5076269.
22. Cui, X.; Wang, N.; Zhao, Y.; Chen, S.; Li, S.; Xu, M.; Chai, R. Preoperative Prediction of Axillary Lymph Node Metastasis in Breast Cancer Using Radiomics Features of DCE-MRI. Sci. Rep. 2019, 9, 2240, doi:10.1038/s41598-019-38502-0.
23. Yang, J.; Wang, T.; Yang, L.; Wang, Y.; Li, H.; Zhou, X.; Zhao, W.; Ren, J.; Li, X.; Tian, J.; et al. Preoperative Prediction of Axillary Lymph Node Metastasis in Breast Cancer Using Mammography-Based Radiomics Method. Sci. Rep. 2019, 9, 4429, doi:10.1038/s41598-019-40831-z.
24. Tirada, N.; Aujero, M.; Khorjekar, G.; Richards, S.; Chopra, J.; Dromi, S.; Ioffe, O. Breast Cancer Tissue Markers, Genomic Profiling, and Other Prognostic Factors: A Primer for Radiologists. Radiogr. Rev. Publ. Radiol. Soc. N. Am. Inc 2018, 38, 1902–1920, doi:10.1148/rg.2018180047.
25. Gradishar, W.J.; Anderson, B.O.; Balassanian, R.; Blair, S.L.; Burstein, H.J.; Cyr, A.; Elias, A.D.; Farrar, W.B.; Forero, A.; Giordano, S.H.; et al. Breast Cancer, Version 4.2017, NCCN Clinical Practice Guidelines in Oncology. J. Natl. Compr. Cancer Netw. JNCCN 2018, 16, 310–320, doi:10.6004/jnccn.2018.0012.
26. Torre, L.A.; Siegel, R.L.; Ward, E.M.; Jemal, A. Global Cancer Incidence and Mortality Rates and Trends--An Update. Cancer Epidemiol. Biomark. Prev. Publ. Am. Assoc. Cancer Res. Cosponsored Am. Soc. Prev. Oncol. 2016, 25, 16–27, doi:10.1158/1055-9965.EPI-15-0578.
27. Tagliafico, A.S.; Piana, M.; Schenone, D.; Lai, R.; Massone, A.M.; Houssami, N. Overview of Radiomics in Breast Cancer Diagnosis and Prognostication. Breast Edinb. Scotl. 2020, 49, 74–80, doi:10.1016/j.breast.2019.10.018.
28. De Luca, F.; Rotunno, G.; Salvianti, F.; Galardi, F.; Pestrin, M.; Gabellini, S.; Simi, L.; Mancini, I.; Vannucchi, A.M.; Pazzagli, M.; et al. Mutational Analysis of Single Circulating Tumor Cells by next Generation Sequencing in Metastatic Breast Cancer. Oncotarget 2016, 7, 26107–26119, doi:10.18632/oncotarget.8431.
29. Pesapane, F.; Rotili, A.; Agazzi, G.M.; Botta, F.; Raimondi, S.; Penco, S.; Dominelli, V.; Cremonesi, M.; Jereczek-Fossa, B.A.; Carrafiello, G.; et al. Recent Radiomics Advancements in Breast Cancer: Lessons and Pitfalls for the Next Future. Curr. Oncol. Tor. Ont 2021, 28, 2351–2372, doi:10.3390/curroncol28040217.
30. Ogston, K.N.; Miller, I.D.; Payne, S.; Hutcheon, A.W.; Sarkar, T.K.; Smith, I.; Schofield, A.; Heys, S.D. A New Histological Grading System to Assess Response of Breast Cancers to Primary Chemotherapy: Prognostic Significance and Survival. Breast Edinb. Scotl. 2003, 12, 320–327, doi:10.1016/s0960-9776(03)00106-1.
31. Magny, S.J.; Shikhman, R.; Keppke, A.L. Breast Imaging Reporting and Data System. In StatPearls; StatPearls Publishing: Treasure Island (FL), 2023.
32. Strzelecki, M.; Szczypinski, P.; Materka, A.; Klepaczko, A. A Software Tool for Automatic Classification and Segmentation of 2D/3D Medical Images. Nucl. Instrum. Methods Phys. Res. Sect. Accel. Spectrometers Detect. Assoc. Equip. 2013, 702, 137–140, doi:10.1016/j.nima.2012.09.006.
33. Jensen, L.J.; Kim, D.; Elgeti, T.; Steffen, I.G.; Hamm, B.; Nagel, S.N. Stability of Radiomic Features across Different Region of Interest Sizes-A CT and MR Phantom Study. Tomogr. Ann Arbor Mich 2021, 7, 238–252, doi:10.3390/tomography7020022.
34. Gity, M.; Moradi, B.; Arami, R.; Arabkheradmand, A.; Kazemi, M.A. Two Different Methods of Region-of-Interest Placement for Differentiation of Benign and Malignant Breast Lesions by Apparent Diffusion Coefficient Value. Asian Pac. J. Cancer Prev. APJCP 2018, 19, 2765–2770, doi:10.22034/APJCP.2018.19.10.2765.

35. Holli, K.; Lääperi, A.-L.; Harrison, L.; Luukkaala, T.; Toivonen, T.; Ryymin, P.; Dastidar, P.; Soimakallio, S.; Eskola, H. Characterization of Breast Cancer Types by Texture Analysis of Magnetic Resonance Images. Acad. Radiol. 2010, 17, 135–141, doi:10.1016/j.acra.2009.08.012.
36. Nicosia, L.; Bozzini, A.C.; Ballerini, D.; Palma, S.; Pesapane, F.; Raimondi, S.; Gaeta, A.; Bellerba, F.; Origgi, D.; Marco, P. Radiomic Features Applied to Contrast Enhancement Spectral Mammography: Possibility to Predict Breast Cancer Molecular Subtypes in a Non-Invasive Manner. Int J Mol Sci 2022, 23, 15322.
37. Pesapane, F.; De Marco, P.; Rapino, A.; Lombardo, E.; Nicosia, L.; Tantrige, P.; Rotili, A.; Bozzini, A.C.; Penco, S.; Dominelli, V.; et al. How Radiomics Can Improve Breast Cancer Diagnosis and Treatment. J. Clin. Med. 2023, 12, 1372, doi:10.3390/jcm12041372.
38. Yip, S.S.F.; Parmar, C.; Kim, J.; Huynh, E.; Mak, R.H.; Aerts, H. Impact of Experimental Design on PET Radiomics in Predicting Somatic Mutation Status. Eur J Radiol 2017, 97, 8–15.
39. Saravi, B.; Zink, A.; Ülkümen, S.; Couillard-Despres, S.; Wollborn, J.; Lang, G.; Hassel, F. Clinical and Radiomics Feature-Based Outcome Analysis in Lumbar Disc Herniation Surgery. BMC Musculoskelet. Disord. 2023, 24, 791, doi:10.1186/s12891-023-06911-y.
40. Saravi, B. and H., F. and Ülkümen, S. and Zink, A. and Shavlokhova, V. and Couillard-Despres, S. and Boeker, M. and Obid, P. and Lang, G.M. Artificial Intelligence-Driven Prediction Modeling and Decision Making in Spine Surgery Using Hybrid Machine Learning Models. J Med 2022, 12, 509.
41. Pesapane, F.; Codari, M.; Sardanelli, F. Artificial Intelligence in Medical Imaging: Threat or Opportunity? Radiologists Again at the Forefront of Innovation in Medicine. Eur Radiol Exp 2018, 2, 35.
42. Bevers, T.B.; Helvie, M.; Bonaccio, E.; Calhoun, K.E.; Daly, M.B.; Farrar, W.B.; Garber, J.E.; Gray, R.; Greenberg, C.C.; Greenup, R. Breast Cancer Screening and Diagnosis, Version 3.2018, NCCN Clinical Practice Guidelines in Oncology. J Natl Compr Cancer Netw 2018, 16, 1362–1389.
43. Zhou, J.; Zhang, Y.; Chang, K.T.; Lee, K.E.; Wang, O.; Li, J.; Lin, Y.; Pan, Z.; Chang, P.; Chow, D. Diagnosis of Benign and Malignant Breast Lesions on DCE-MRI by Using Radiomics and Deep Learning With Consideration of Peritumor Tissue. J Magn Reson Imaging 2019, 51, 798–809.
44. Xie, T.; Wang, Z.; Zhao, Q.; Bai, Q.; Zhou, X.; Gu, Y.; Peng, W. Machine Learning-Based Analysis of MR Multiparametric Radiomics for the Subtype Classification of Breast Cancer. Front Oncol 2019, 9, 505.
45. Li, H.; Mendel, K.R.; Lan, L.; Sheth, D.; Giger, M.L. Digital Mammography in Breast Cancer: Additive Value of Radiomics of Breast Parenchyma. Radiology 2019, 291, 15–20.
46. Bickelhaupt, S.; Jaeger, P.F.; Laun, F.B.; Lederer, W.; Daniel, H.; Kuder, T.A.; Wuesthof, L.; Paech, D.; Bonekamp, D.; Radbruch, A. Radiomics Based on Adapted Diffusion Kurtosis Imaging Helps to Clarify Most Mammographic Findings Suspicious for Cancer. Radiology 2018, 287, 761–770.
47. Tagliafico, A.S.; Valdora, F.; Mariscotti, G.; Durando, M.; Nori, J.; Forgia, D.; Rosenberg, I.; Caumo, F.; Gandolfo, N.; Houssami, N. An Exploratory Radiomics Analysis on Digital Breast Tomosynthesis in Women with Mammographically Negative Dense Breasts. Breast 2018, 40, 92–96.
48. Luo, W.Q.; Huang, Q.X.; Huang, X.W.; Hu, H.T.; Zeng, F.Q.; Wang, W. Predicting Breast Cancer in Breast Imaging Reporting and Data System (BI-RADS) Ultrasound Category 4 or 5 Lesions: A Nomogram Combining Radiomics and BI-RADS. Sci Rep 2019, 9, 11921.
49. Fan, M.; Li, H.; Wang, S.; Zheng, B.; Zhang, J.; Li, L. Radiomic Analysis Reveals DCE-MRI Features for Prediction of Molecular Subtypes of Breast Cancer. PLoS ONE 2017, 12, 0171683.
50. Xie, T.; Zhao, Q.; Fu, C.; Bai, Q.; Zhou, X.; Li, L.; Gu, Y.; Peng, W. Differentiation of Triple-Negative Breast Cancer from Other Subtypes through Whole-Tumor Histogram Analysis on Multiparametric MR Imaging. Eur Radiol 2019, 29, 2535–2544.
51. Demircioglu, A.; Grueneisen, J.; Ingenwerth, M.; Hoffmann, O.; Pinker-Domenig, K.; Morris, E.; Haubold, J.; Forsting, M.; Nensa, F.; Umutlu, L. A Rapid Volume of Interest-Based Approach of Radiomics Analysis of Breast MRI for Tumor Decoding and Phenotyping of Breast Cancer. PLoS ONE 2020, 15, 0234871.
52. Pesapane, F.; Agazzi, G.M.; Rotili, A.; Ferrari, F.; Cardillo, A.; Penco, S.; Dominelli, V.; D'Ecclesiis, O.; Vignati, S.; Raimondi, S. Prediction of the Pathological Response to Neoadjuvant Chemotherapy in Breast Cancer Patients With MRI-Radiomics: A Systematic Review and Meta-Analysis. Curr Probl Cancer 2022, 46, 100883.
53. Pesapane, F.; Rotili, A.; Botta, F.; Raimondi, S.; Bianchini, L.; Corso, F.; Ferrari, F.; Penco, S.; Nicosia, L.; Bozzini, A. Radiomics of MRI for the Prediction of the Pathological Response to Neoadjuvant Chemotherapy in Breast Cancer Patients: A Single Referral Centre Analysis. Cancers 2021, 13, 4271.

54. Braman, N.M.; Etesami, M.; Prasanna, P.; Dubchuk, C.; Gilmore, H.; Tiwari, P.; Plecha, D.; Madabhushi, A. Intratumoral and Peritumoral Radiomics for the Pretreatment Prediction of Pathological Complete Response to Neoadjuvant Chemotherapy Based on Breast DCE-MRI. Breast Cancer Res 2017, 19, 57.
55. Choudhery, S.; Gomez-Cardona, D.; Favazza, C.P.; Hoskin, T.L.; Haddad, T.C.; Goetz, M.P.; Boughey, J.C. MRI Radiomics for Assessment of Molecular Subtype, Pathological Complete Response, and Residual Cancer Burden in Breast Cancer Patients Treated With Neoadjuvant Chemotherapy. Acad Radiol 2020, 29, 145–154.
56. Fan, M.; Wu, G.; Cheng, H.; Zhang, J.; Shao, G.; Li, L. Radiomic Analysis of DCE-MRI for Prediction of Response to Neoadjuvant Chemotherapy in Breast Cancer Patients. Eur J Radiol 2017, 94, 140–147.
57. Ahmed, A.; Gibbs, P.; Pickles, M.; Turnbull, L. Texture Analysis in Assessment and Prediction of Chemotherapy Response in Breast Cancer. J Magn Reson Imaging 2013, 38, 89–101.
58. Galimberti, V.; Cole, B.F.; Viale, G.; Veronesi, P.; Vicini, E.; Intra, M.; Mazzarol, G.; Massarut, S.; Zgajnar, J.; Taffurelli, M. Axillary Dissection versus No Axillary Dissection in Patients with Breast Cancer and Sentinel-Node Micrometastases (IBCSG 23-01): 10-Year Follow-up of a Randomised, Controlled Phase 3 Trial. Lancet Oncol 2018, 19, 1385–1393.
59. Hieken, T.J.; Trull, B.C.; Boughey, J.C.; Jones, K.N.; Reynolds, C.A.; Shah, S.S.; Glazebrook, K.N. Preoperative Axillary Imaging with Percutaneous Lymph Node Biopsy Is Valuable in the Contemporary Management of Patients with Breast Cancer. Surgery 2013, 154, 831–838.
60. Tan, H.; Wu, Y.; Bao, F.; Zhou, J.; Wan, J.; Tian, J.; Lin, Y.; Wang, M. Mammography-Based Radiomics Nomogram: A Potential Biomarker to Predict Axillary Lymph Node Metastasis in Breast Cancer. Br J Radiol 2020, 93, 20191019.
61. Yu, Y.; Tan, Y.; Xie, C.; Hu, Q.; Ouyang, J.; Chen, Y.; Gu, Y.; Li, A.; Lu, N.; He, Z. Development and Validation of a Preoperative Magnetic Resonance Imaging Radiomics-Based Signature to Predict Axillary Lymph Node Metastasis and Disease-Free Survival in Patients With Early-Stage Breast Cancer. JAMA Netw Open 2020, 3, 2028086.
62. Mao, N.; Yin, P.; Li, Q.; Wang, Q.; Liu, M.; Ma, H.; Dong, J.; Che, K.; Wang, Z.; Duan, S. Radiomics Nomogram of Contrast-Enhanced Spectral Mammography for Prediction of Axillary Lymph Node Metastasis in Breast Cancer: A Multicenter Study. Eur Radiol 2020, 30, 6732–6739.
63. Cattell, R.; Ying, J.; Lei, L.; Ding, J.; Chen, S.; Serrano Sosa, M.; Huang, C. Preoperative Prediction of Lymph Node Metastasis Using Deep Learning-Based Features. Vis Comput Ind Biomed Art 2022, 5, 8.
64. Fisher, B.; Jeong, J.H.; Anderson, S.; Bryant, J.; Fisher, E.R.; Wolmark, N. Twenty-Five-Year Follow-up of a Randomized Trial Comparing Radical Mastectomy, Total Mastectomy, and Total Mastectomy Followed by Irradiation. N. Engl J Med 2002, 347, 567–575.
65. Park, H.; Lim, Y.; Ko, E.S.; Cho, H.H.; Lee, J.E.; Han, B.K.; Choi, J.S.; Park, K.W. Radiomics Signature on Magnetic Resonance Imaging: Association with Disease-Free Survival in Patients with Invasive Breast Cancer. Clin Cancer Res 2018, 24, 4705–4714.
66. Chitalia, R.D.; Rowland, J.; McDonald, E.S.; Pantalone, L.; Cohen, E.A.; Gastounioti, A.; Feldman, M.; Schnall, M.; Conant, E.; Kontos, D. Imaging Phenotypes of Breast Cancer Heterogeneity in Preoperative Breast Dynamic Contrast Enhanced Magnetic Resonance Imaging (DCE-MRI) Scans Predict 10-Year Recurrence. Clin Cancer Res 2020, 26, 862–869.
67. Mazurowski, M.A.; Saha, A.; Harowicz, M.R.; Cain, E.H.; Marks, J.R.; Marcom, P.K. Association of Distant Recurrence-Free Survival with Algorithmically Extracted MRI Characteristics in Breast Cancer. J Magn Reson Imaging 2019, 49, 231–240.
68. Xiong, L.; Chen, H.; Tang, X.; Chen, B.; Jiang, X.; Liu, L.; Feng, Y.; Liu, L.; Li, L. Ultrasound-Based Radiomics Analysis for Predicting Disease-Free Survival of Invasive Breast Cancer. Front Oncol 2021, 11, 621993.
69. Yu, F.; Hang, J.; Deng, J.; Yang, B.; Wang, J.; Ye, X.; Liu, Y. Radiomics Features on Ultrasound Imaging for the Prediction of Disease-Free Survival in Triple Negative Breast Cancer: A Multi-Institutional Study. Br J Radiol 2021, 94, 20210188.
70. Dasgupta, A.; Bhardwaj, D.; DiCenzo, D.; Fatima, K.; Osapoetra, L.O.; Quiaoit, K.; Saifuddin, M.; Brade, S.; Trudeau, M.; Gandhi, S. Radiomics in Predicting Recurrence for Patients with Locally Advanced Breast Cancer Using Quantitative Ultrasound. Oncotarget 2021, 12, 2437–2448.
71. Mao, N.; Yin, P.; Zhang, H.; Zhang, K.; Song, X.; Xing, D.; Chu, T. Mammography-Based Radiomics for Predicting the Risk of Breast Cancer Recurrence: A Multicenter Study. Br J Radiol 2021, 94, 20210348.